ISSN 0040-6015, Thermal Engineering, 2013, Vol. 60, No. 4, pp. 285–294. © Pleiades Publishing, Inc., 2013.
Original Russian Text © I.A. Popov, N.N. Zubkov, S.I. Kas'kov, A.V. Shchelchkov, 2013, published in Teploenergetika.

HEAT AND MASS TRANSFER AND PROPERTIES OF WORKING FLUIDS AND MATERIALS

Heat Transfer during the Boiling of Liquid on Microstructured Surfaces. Part 2: Visualization of Boiling and Critical Heat Fluxes

I. A. Popov[a], N. N. Zubkov[b], S. I. Kas'kov[b], and A. V. Shchelchkov[a]

[a] *Tupolev Kazan National Research Technical University, ul. K. Marksa 10, Kazan, 420111 Russia*
[b] *Bauman Moscow State Technical University, Vtoraya Baumanskaya ul. 5, Moscow, 105005 Russia*

Abstract—Results from visualization of boiling process and experimental study of critical heat fluxes on microstructured surfaces are presented. The studied surfaces were obtained using the deforming cutting method and have different design shapes and sizes. Mechanisms of heat transfer enhancement are substantiated. A factor of 4.1 higher value of critical heat flux is obtained.

Keywords: pool boiling, heat transfer enhancement, critical heat flux, visualization

DOI: 10.1134/S0040601513040113

Nucleate boiling is the main kind of two-phase heat transfer during which heat is transferred from a heated wall to liquid heated to the saturation temperature at the place in which they come in contact with each other. This two-phase transfer process is characterized by significant heat-transfer coefficients due to an intense phase transformation process. The intensity of heat-transfer process is governed by the dynamics with which a steam bubble is generated, grows, and separates from the heated surface.

The following tasks are to be solved in enhancing boiling heat transfer [1–7]. First, it is necessary to achieve the onset of nucleate boiling at a smaller difference of temperatures between the hot wall and liquid and obtain high heat-transfer coefficients in this zone. Second, it is necessary to increase the critical heat flux that identifies the onset of burnout, i.e., to widen the nucleate boiling region.

The first task is solved by applying capillary-porous coatings. However, the use of this approach gives insufficiently high critical heat fluxes. Higher critical fluxes are achieved through the use of microstructured surfaces obtained by subjecting them to mechanical processing or to small-scale deformations of the surface. Such surfaces are used primarily for boiling processes with natural convection [5, 6]. Enhancement of boiling heat transfer on microstructured surfaces is widely used in cooling systems and in heat-transfer equipment [8].

In [9], the results from a study of heat transfer during boiling of distilled water on microstructured surfaces obtained using the deforming cutting method were presented. The greatest enhancement of heat transfer was achieved for surfaces with 3D columnar and channel structures: by a factor of 3 to 9. The heat-transfer enhancement ratio obtained for 2D microfins was up to 2.5.

In this work, the results from visualization of boiling on the studied microstructured surfaces are presented and intermediate results from a study of critical heat fluxes are discussed.

METHODS FOR SHAPING BOILING SURFACES

Surfaces obtained using the deforming cutting method (DCM), which implies a combined use of partial cutting and bending of the surface layers of a heat transfer surface [10–14], can be used as microstructured surfaces for enhancement of boiling processes.

The totality of partially cut and plastically deformed layers, which retained the continuity of their connection with the billet, forms an extended microrelief on the treated surface. The DCM is embodied by using standard metal cutting equipment, including that with numerical program control and is a waste-free and high-efficient process, and allows all geometrical characteristics of the obtained macrorelief to be controlled. Interfin gaps with sizes ranging from a few micrometers to a few millimeters can be obtained. The degree to which this process can be realized in practice depends in the main on the plasticity of material being processed and on the cutting depth to supply ratio. For materials with relative elongation of more than 30% (the majority of nonferrous metals fall under this category), the height of fins may be up to 7 finning pitches (Fig. 1a), but no more than 4 mm. For materials with relative elongation ranging from 20 to 30% (this category encompasses the majority of

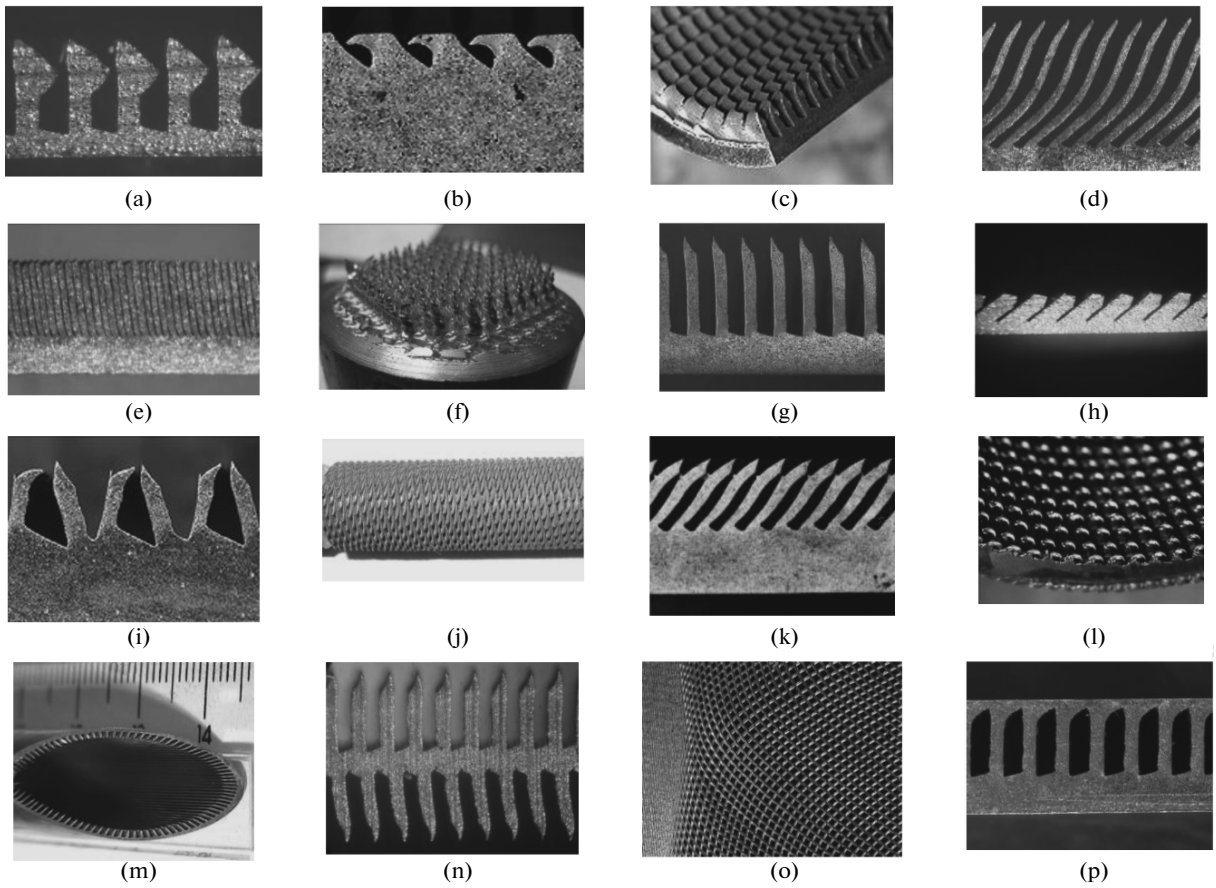

Fig. 1. Structured surfaces of different configurations obtained using the deforming cutting method. (a), (b), (i), and (p) Structures with inner steam cavities; (j) cellular structures; (c), (f), and (l) micropin structures; (e), g), (m), and (n) finned 2D and 3D structures with a microgap between the fins; (d), (h), and (k) inclined finned microstructures; and (o) microgrids attached to the boiling surface.

steels), the maximal height of fins is 3–5 finning pitches. Materials with relative elongation of less than 18% do not lend themselves to processing by deforming cutting. For nonferrous metals, the surface area obtained after processing it using the DCM can be increased by as much as a factor of 14. Some versions of structured surfaces obtained using the DCM are shown in Fig. 1.

Two-dimension structures with inner steam cavities can be obtained using the DCM either in one or two passes of a tool the cutting or deforming edge of which has special configuration (see Figs. 1a, 1b). Finning like that shown in Fig. 1g is formed first, followed by plastically deforming the fin tips, e.g., by subjecting them to smoothing or knurling with a smooth or corrugated roller. Steam cavities can also be obtained by using bifilar finning with different slopes of fins in the neighboring passes (see Fig. 1i).

Three-dimensional micropin (columnar) structures can be obtained either by shaping fins on the billet surface in noncoinciding directions and by applying corrugation prior to subject the surface to the deforming cutting operation. In this case, corrugations play the role of stress concentrators, due to which partial or full breaks of fins along their height are obtained to form pin structures (see Figs. 1c, 1l). By subjecting the structures to subsequent smoothing or rolling with a smooth roller, 3D structures with subsurface cavities can be obtained.

The mechanism through which cellular structures are generated using the deforming cutting method (see Fig. 1j) has been disclosed only partially; nonetheless, it can be stated that this structure, which is obtained in one pass of the tool, is a system of "microbowls" on the boiling surface, which were not known before in the relevant engineering practices around the world.

The deforming cutting method does not have any limitations of fundamental nature on the minimal width of interfin gaps. With the equal angles of the cutting and deforming edges in a horizontal plane, the finning will have an interfin gap commensurable with the roughness of the fin lateral walls (see Fig. 1e). In

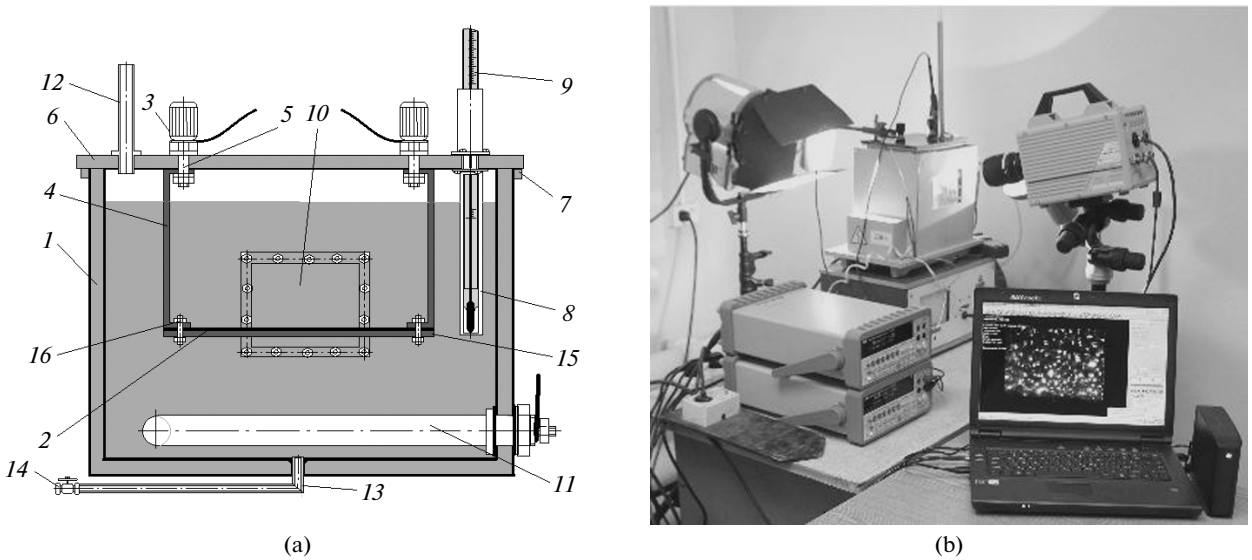

(a) (b)

Fig. 2. (a) Basic process circuit and (b) external view of the experimental setup. (*1*) Heat-insulated housing, (*2*) studied sample, (*3*) terminals, (*4*) current inlets, (*5*) threaded joint, (*6*) cover, (*7*) collar, (*8*) casing, (*9*) thermometer, (*10*) inspection window, (*11*) tubular electric heater, (*12*) condenser sleeve, (*13*) drain socket, (*14*) valve, (*15*) textolite base for the sample, and (*16*) fastener.

using the DCM, the interfin gap can be easily adjusted from densely packed fins (from a few to a few tens of micrometers) to a few millimeters. Such structures were not investigated before. Inclined finning (see Figs. 1h, 1j, 1k) is shaped by the tool used for the DCM with an auxiliary angle in a horizontal plane different from 90°. By using the DCM, it is possible to obtain microgrids from thin-sheet billets (see Fig. 1o)

Parameters of the studied plates

No. of sample (Fig. 3)	Material	Fin height h, μm	Fin pitch s, μm	Interfin gap b, μm	Fin angle, deg	Dimple depth, mm	Dimple diameter, mm	Knurling pitch, μm	Groove width, μm
1, 2	12Kh18N9T steel	–	–	–	–	–	–	–	–
3	12Kh18N9T steel	–	–	–	–	1	2	–	–
4	12Kh18N9T steel	–	–	–	–	0.5	1	–	–
5	VT1-00	95	40	15	3	–	–	–	–
6	VT1-00	310	160	63	3	–	–	–	–
7	VT1-00	200	120	46	3	–	–	–	–
8	VT1-00	230	90	35	3	–	–	–	–
9	VT1-00	220	60	22	3	–	–	–	–
10	AISI 1020	420	350	–	0	–	–	318	140
11	12Kh18N10T steel	150	160	50	0	–	–	–	–
12	12Kh18N10T steel	90	160	50	0	–	–	–	–
13	VT1-00	200	200	30–40	30	–	–	–	–
14	12Kh18N10T steel	200	160	50	0	–	–	–	–
15	AISI 1020	340	240	–	15	–	–	318	140
16	12Kh18N10T steel	200	160	50	0	–	–	–	–

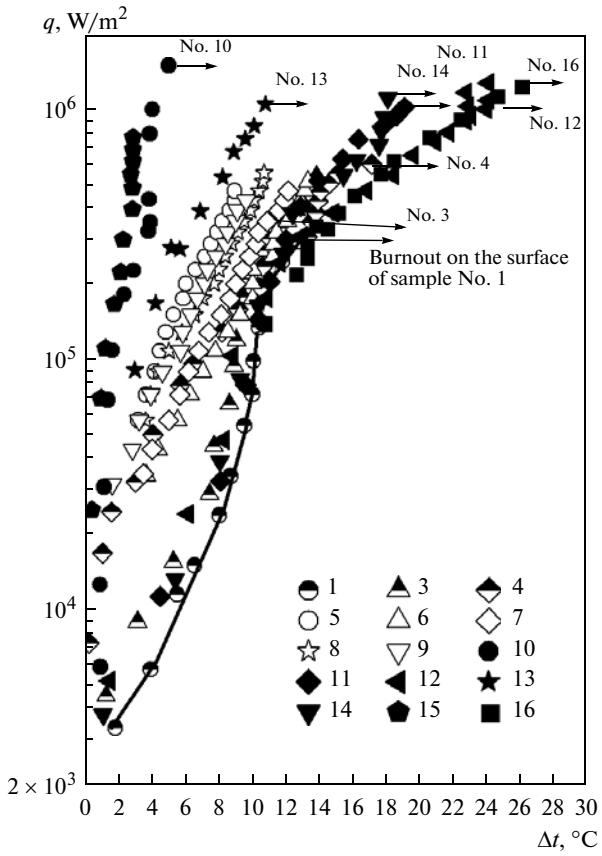

Fig. 3. Heat fluxes during the boiling of water on the surfaces of samples with different configurations. (1–16) are the numbers of samples (see the table).

that may cover heat-transfer surfaces. These grids have a surface area several times larger than that of wire coatings, and the characteristic size of interfin gaps may be in the range from a few to a few tens of micrometers.

EXPERIMENTAL SETUP AND MEASUREMENT PROCEDURE

The experimental investigations were carried out on a setup the model of which is shown in Fig. 2. The description of the setup, test conditions, and procedure for carrying out the tests were presented in [9].

The boiling process was visualized by means of a Photron Fastcam SA4-500K-C1 high-speed video camera fitted with Nikon AF 60 mm F/2.8 D Micro and Navitar DO-2595 (25 mm F/0.95) optical systems, using which video recording of the process can be performed during an experiment at a frame rate of 3000–20 000 shots/s. The visualized process was lit using a 1-kW ARRI ST1 lighting installation fitted with a 175-mm Fresnel lens and a Schott DCR III local fiber-optic lighting system with a 150-W EKE lamp.

The heat flux density and the heat transfer coefficient were calculated from the following formulas:

$$q = Q/F = I\Delta U/F; \quad \alpha = Q/(F\Delta t),$$

where α is the heat transfer coefficient, W/(m^2 K); F is the surface area of the plate on which fins are applied (without taking into account its increase as a result of finning), m^2; Q is the heat flux releasing on the plate, W; I is the current fed to the plate, A; ΔU is the voltage drop across the plate, V; and $\Delta t = \bar{t}_{wl} - t_{wt}$ is the difference between the average sample surface temperature and water temperature, K.

Descriptions of the studied samples are given in [9]. The characteristic sizes of boiling heat transfer intensifiers are given in the table.

The data for samples Nos. 5–9 were obtained by a team of scientists led by M.D. Diev; D.N. Morskoi and A.A. Yakomaskin continue the works [15, 16].

STUDY RESULTS

Visualization of the boiling process. The experimental data were obtained for water at atmospheric pressure. Heat flux was varied in the range from 10 to

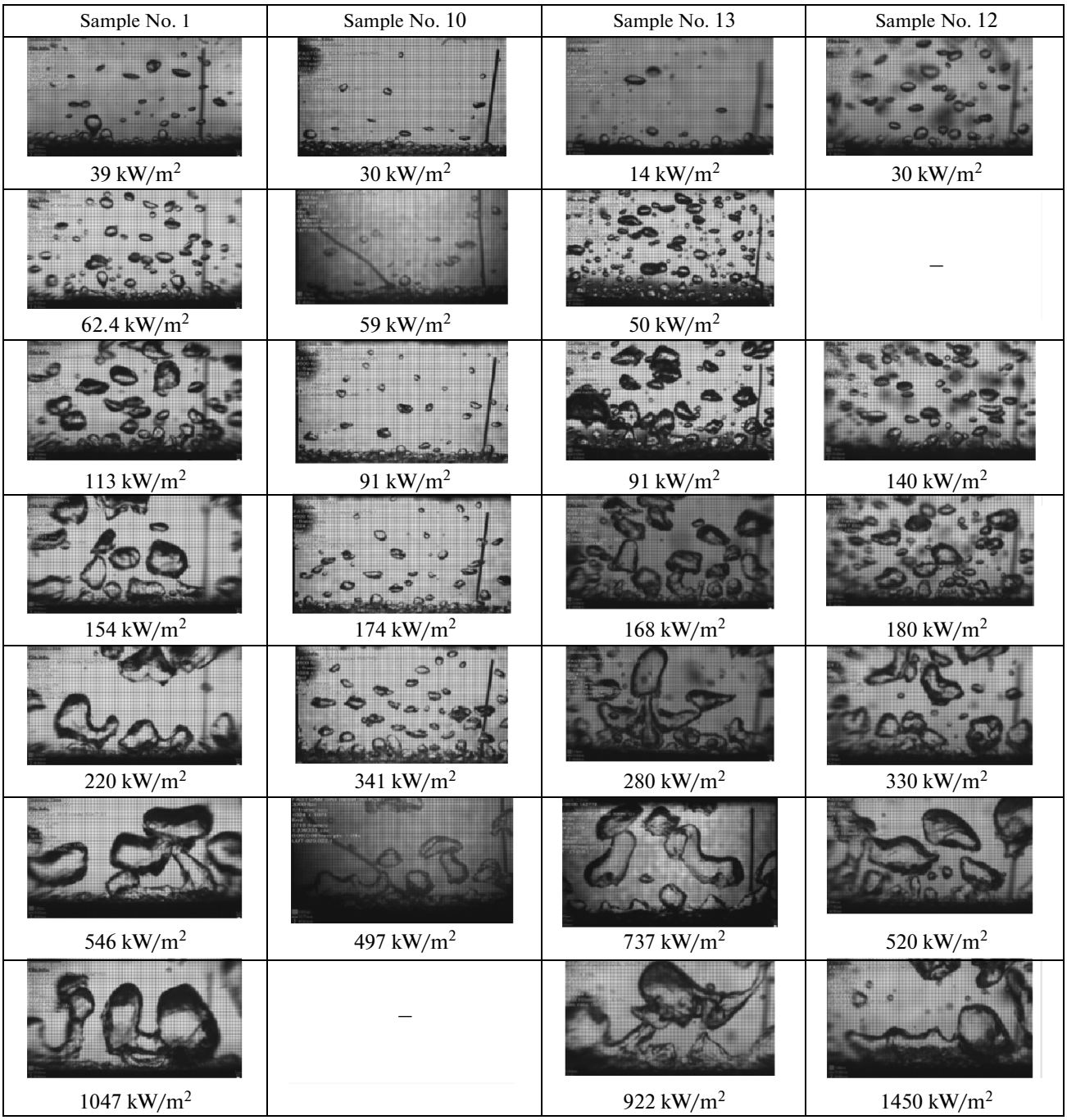

Fig. 4. Bubble generation intensity in boiling on different heat-transfer surfaces (the grid sell size on the photographs is 1 × 1 mm).

1200 kW/m^2. Surface boiling, developed nucleate boiling, and burnout modes were observed in the studied range of heat flux densities. The investigations were carried out in a boiling mode when the temperature of liquid in the boiling chamber in the zone of experimental samples was 97.5–99.3°C. In [9] it was shown that the results of test experiments for boiling of water on a smooth surface are in good agreement with the results of calculation carried out using D.A. Labuntsov's dependence $\alpha = 3q^{0.7}p^{0.1}$.

It follows from [9] that application of surfaces with a relief obtained using the deforming cutting method makes it possible to achieve higher heat-transfer coefficients at a preset difference of temperatures between the wall and liquid, and to obtain the onset of nucleate

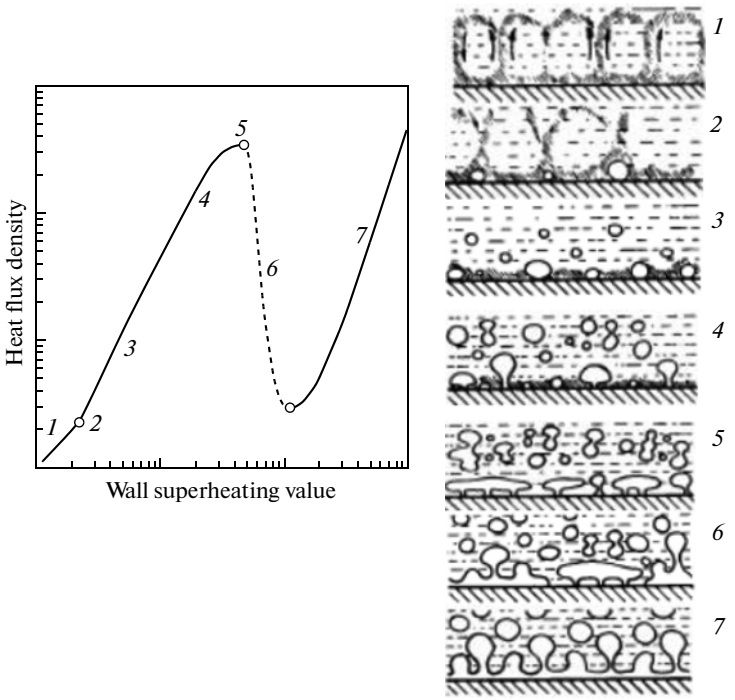

Fig. 5. Boiling curve and characteristic boiling modes [1]. (*1*) Free convection, (*2*) onset of boiling, (*3*) nucleate boiling at low heat fluxes, (*4*) nucleate boiling at high heat fluxes, (*5*) burnout, (*6*) transition boiling, and (*7*) film boiling.

boiling at smaller differences of temperatures between the hot wall and liquid.

The highest heat transfer enhancement ratio is observed for surfaces with 3D columnar microroughness (samples Nos. 15 and 10), the value of which varies from 4.5 to 9 depending on the heat flux density. A heat transfer enhancement ratio equal to 2.5–3.0 was achieved in sample No. 3 having continuous fins the horizontally bent ends of which form microchannels. The results obtained for the surfaces of samples Nos. 5–9, 11, 12, 14, and 16 with 2D microfins were analyzed, and it was found from that analysis that the heat transfer enhancement ratio varied from 1.0 to 2.5 as compared with a smooth surface. It was also found that the heat-transfer coefficients obtained for sample No. 14 with longitudinal heat-releasing fins were 8–50% higher than in sample No. 16 with transverse heat-dissipating fins of the same shape and sizes.

The main mechanism through which heat transfer is enhanced on all of the considered surfaces involves a growth of nucleation sites and persistence of microbubbles in the interfin space in the boiling development process, decrease of steam bubble diameter at the moment of its separation, and increase of separation frequency.

For substantiating the mechanisms of heat transfer enhancement on the studied surfaces, video recording of the boiling process on the samples was performed in the course of experiments. Figure 4 shows how the boiling process evolves on samples Nos. 1, 10, 13, and 12. The heat flux values are indicated under the photographs. Visualization of the boiling process for the surfaces of samples Nos. 1, 3, and 9 is presented in [17]. The boiling processes were recorded mainly at a rate of 3000–4500 shots/s with a resolution of 1024 × 800.

The visualization results shown in Fig. 4 are in good consistency with the existing boiling mode models [1] (Fig. 5).

In Fig. 3 we see the data showing how heat fluxes depend on the superheating of heat transfer surface. It is well seen from this figure that higher heat-transfer coefficients, earlier onset of boiling, and higher critical heat fluxes are obtained on the considered surfaces as a result of heat transfer enhancement.

The onset of boiling on the smooth surface of sample No. 1 occurs at the surface superheating value Δt equal to around 4°C. For the surfaces of samples Nos. 10, 13, and 15 featuring significant enhancement of heat transfer, the onset of boiling corresponds to $\Delta t \approx 0.3$–0.5°C. For the surfaces of samples Nos. 4–9, the onset of boiling also occurs earlier than on a smooth surface and corresponds to $\Delta t \approx 0.3$–1°C. The onset of boiling on the surfaces of samples Nos. 11, 12, 14, and 16 occurs under approximately the same conditions as on smooth surfaces: at $\Delta t \approx 3$–4°C.

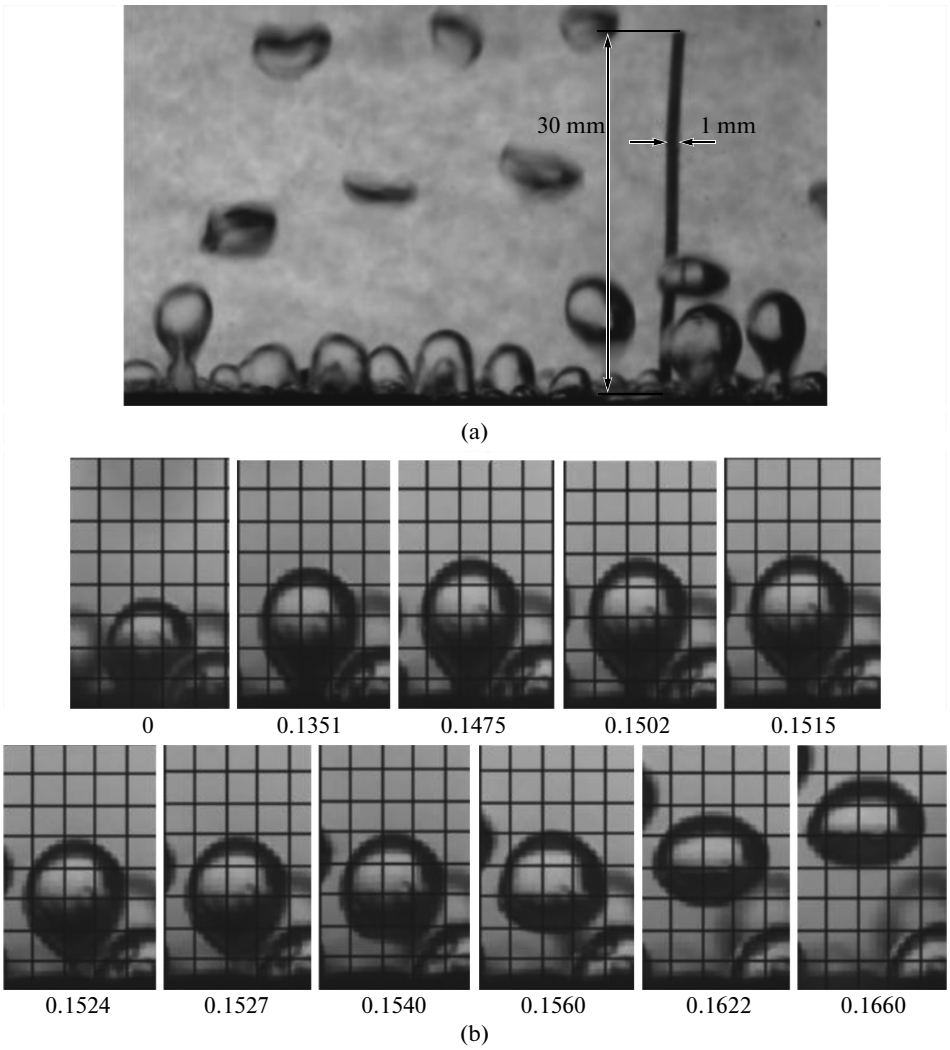

Fig. 6. Shapes of bubbles on the boiling surfaces. Surface of sample: (a) No. 1 and (b) No. 12 (the grid size is 1 × 1 mm). The numbers under the figures indicate the time in seconds.

The results of visualization showed that the boiling processes on surfaces obtained using the DCM are characterized by a larger number of nucleation sites, smaller bubble diameters at the bubble separation moment, and a higher bubble separation frequency. The above-mentioned features are especially the case on the surfaces of samples Nos. 10, 13, and 15, on which a drastically smaller diameter of separating bubbles and higher bubble separation frequency are observed.

The bubble separation frequency was not recorded individually, but it can be seen from Fig. 4 that its value is higher on the surfaces obtained using the DCM because the volume of boiling water is saturated with steam bubbles to a higher extent.

No essential difference was observed in the number of nucleation sites on the surfaces of samples Nos. 5–16: it is equal to 0.05–0.1 1/mm^2 at $q = 7.7$–30 kW/m^2 and begins to grow starting from this value to 0.25 1/mm^2 at $q = 40$–80 kW/m^2. However, as we see from the visualization results, a change occurred in the surface wetting angle (Fig. 6). Owing to the "finned" profile, a drastic drop occurred in the wetting angle, which led to a growth of bubble separation frequency and to some decrease of steam bubble diameter at the separation moment. At high heat loads, it was rather difficult to determine the number of nucleation sites on the surfaces due to their higher density and because steam bubbles merged with each other before separation.

From Fig. 7, drawn for a comparative analysis of the patterns in which steam bubble diameters are distributed in the 20-mm-high volume of boiling water above the boiling surface at $q > 220$–313 kW/m^2, we see that the surfaces of samples Nos. 10, 13, and 14 are characterized by smaller steam bubble sizes: the vol-

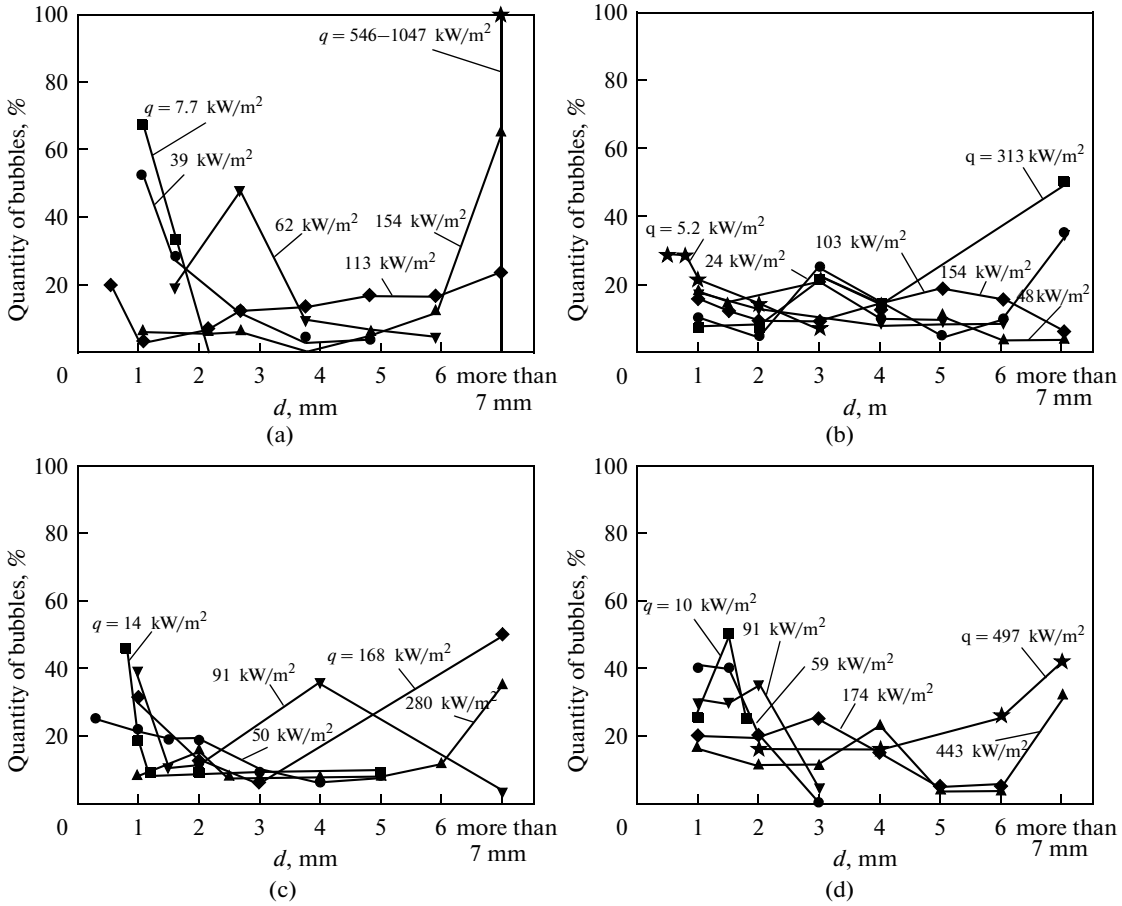

Fig. 7. Distribution of steam bubbles by their diameters in the near-wall zone (20 mm) above the boiling surfaces at different heat flux densities. Surface of sample: (a) No. 1, (b) No. 14, (c) No. 13, and (d) No. 10.

ume of water has approximately the same content (8–25%) of bubbles with diameters from 1 to 6 mm and approximately 35–40% of bubbles with a diameter larger than 7 mm. During the boiling on a smooth surface, the major part of bubbles (66–100%) have diameters more than 7 mm, whereas bubbles 1 and 2 mm in diameter account for 0–25%, and it should be noted that these smaller bubbles are generated due to fracture of larger bubbles when they separate from the boiling surface (film).

Floating bubbles have large diameters because they merge before separation due to a high density of nucleation sites.

Such distribution pattern of bubble diameters and such separation frequency testify that smaller steam bubbles are indeed generated during the boiling on surfaces obtained using the DCM, and that they separate from the surface at higher frequency, due to which more intense heat transfer is achieved. The average bubble floatation velocity in the near-wall zone (with a height of 20 mm) above the boiling surface is shown in Fig. 8. It can be seen that, as the liquid superheating value in the near-wall region increases, so does the floatation velocity. Some decrease in the floatation velocity that is observed at heat loads ranging from 150–400 kW/m^2 above the surfaces obtained using the DCM is due to a large number of steam bubbles and their merging during floatation, which has a decelerating effect.

Critical heat fluxes. The critical heat flux values depending on the geometry of enhanced surfaces were determined (see Fig. 3).

The minimal increase of critical heat fluxes (up to a factor of 2) was obtained on the surfaces of samples Nos. 3 and 4 with macroroughness in the form of a set of spherical dimples. For the surfaces of samples Nos. 11–14 with microroughness in the form of 2D microfins, the critical heat fluxes were increased by a factor of 3.3–4.1. Figure 9 shows that, as the relative height h/Δ of heat-dissipating microfins increases, so do the critical heat fluxes. The surfaces of samples Nos. 14 and 16 with heat-dissipating and heat-releasing microfins of the same height have approximately the same level of critical heat fluxes. However, owing to smaller heat-transfer coefficients, burnout on the surface of sample No. 16 with heat-dissipating micro-

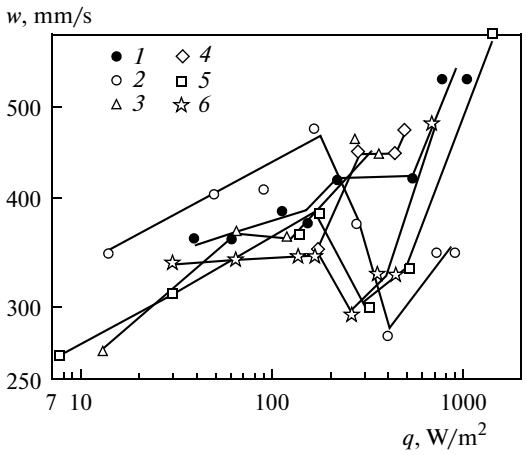

Fig. 8. Average bubble ascending velocity in the 20-mm-high zone above different surfaces during the boiling of water vs. the heat flux density. Surface of sample: (*1*) No. 1, (*2*) No. 13, (*3*) No. 11, (*4*) No. 10, (*5*) No. 12, and (*6*) No. 14.

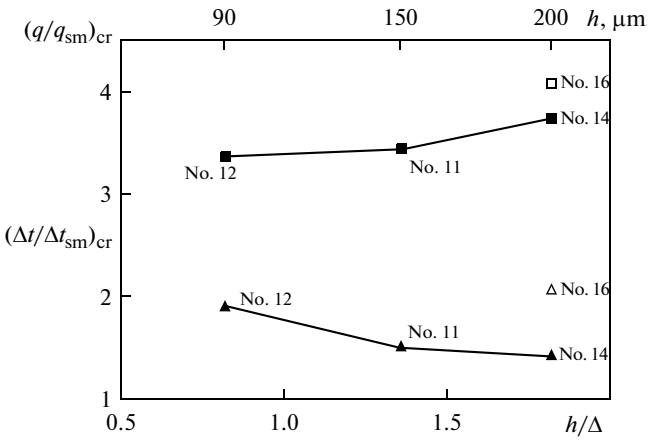

Fig. 9. Influence of microfin height on the critical heat fluxes. $s = 160$ μm, $b = 50$ μm. $\Delta = 110$ μm, $\Delta/b = 2.2$, $s/b = 3.2$; $\varphi = 0$; □, and ■ $(q/q_{sm})_{cr}$, ▲, and △ $[\Delta t/\Delta t_{sm})_{cr}$, ■, and ▲ heat-releasing fins, and □, and △ heat-dissipating fins.

fins occurs at higher differences between the temperatures of surface and liquid. As was pointed out in [9], the average efficiency factor of fins on the surface of sample No. 16 is equal to 0.78, and that for sample No. 14 is equal to 1.0. Thus, the heat transfer coefficients depend partially on the degree of surface extension, and the critical heat fluxes depend in the main on the hydrodynamic pattern of boiling (efficient microcapillary inleakage of liquid through interfin gaps and steam removal [9]).

It was found that burnout on the surfaces of samples Nos. 11, 12, 14, and 16 occurs at higher wall superheating values than on a smooth surface (see Figs. 3, 9). In the studied range of heat flux densities, our attempts to determine the critical heat fluxes for the advanced surface of sample No. 15 were not met with success. The critical heat flux growth ratio obtained for the surface of sample No. 10 with 3D microroughness amounted up to 6 and was due to the presence of zones in which water is sucked to nucleation sites through microchannels between the fins, due to large channels for steam outlet obtained as a result of subjecting the surface to preliminary knurling, and due to a relatively large height of fins.

The onset of burnout was determined from the typical drastic growth of surface temperature accompanied by glowing of the surface, by the occurrence of a break on the graph of specific heat flux vs. the temperature difference, and by a burn-through of the surface (Fig. 10).

Thus, the study results have shown that application of heat-transfer surfaces obtained by using the new resource-saving method for shaping a surface in the form of 2D and 3D microfinned surfaces and channel structures makes it possible to obtain essentially more efficient heat transfer and higher heat fluxes during the

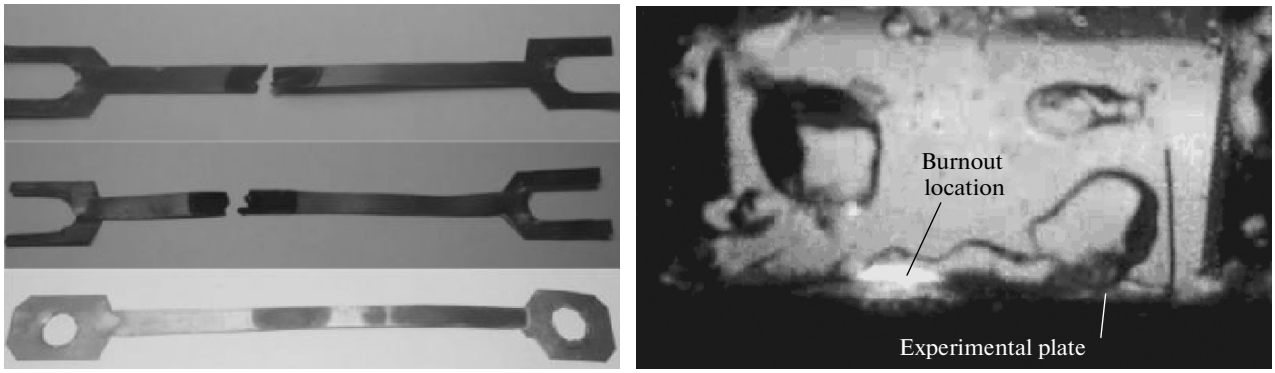

Fig. 10. Experimental plates after burnout and the place of burnout observed during the experiment.

boiling of liquids. The heat flux density has been increased by a factor of 4–6.

REFERENCES

1. M. E. Poniewski and J. R. Thome, *Nucleate Boiling on Micro-Structured Surfaces* (Heat Transfer Research Inc., the United States, 2008).
2. R. L. Webb and N.-H. Kim, *Principles of Enhanced Heat Transfer* (Taylor & Francis Group, New York, 2005).
3. S. Kandlikar, M. Shoji, and V. K. Dhir, *Handbook of Phase Change: Boiling and Condensation* (Taylor & Francis Group, New York, 1999).
4. J. G. Collier and J. R. Thome, *Convective Boiling and Condensation* (Clarendon Press, Oxford, 1994).
5. A. E. Bergles, "Enhancement of Pool Boiling," Int. J. Refrig. **20**, 545 (1997).
6. A. E. Bergles, "Heat Transfer Enhancement – the Encouragement and Accommodation of High Heat Fluxes," J. Heat Transfer **119**, 8 (1997).
7. I. L. Pioro, W. M. Rohsenow, and S. S. Doerffer, "Nucleate Pool Boiling Heat Transfer, 1: Review of Parametric Effects of Boiling Surface," Int. J. Heat & Mass Transfer **47**, 5033 (2004).
8. I. A. Popov, Kh. M. Makhyanov, and V. M. Gureev, *Physical Principles of Heat Transfer Enhancement and Its Industrial Applications: Heat Transfer Enhancement* (Center of Innovative Technologies, Kazan, 2009) [in Russian].
9. I. A. Popov, N. N. Zubkov, S. I. Kas'kov, and A. V. Shchelchkov, "Heat Transfer during the Boiling of Liquid on Microstructured Surfaces. Part 1: Heat Transfer during the Boiling of Water," Therm. Eng., No. 3, (2013).
10. N. N. Zubkov and A. I. Ovchinnikov, "A Method for Obtaining Surfaces with Alternating Protrusions and Recesses and a Tool for Implementing It," RF Patent No. 2044606, Otkr., Izobr., No. 27 (1995).
11. N. N. Zubkov, A. I. Ovchinnikov, and O. V. Kononov, "Fabricating a New Class of Heat-Transfer Surfaces by Deforming Cutting," Vestnik MGTU, No. 4, 79–82 (1993).
12. N. N. Zubkov, "Finning the Tubes of Heat Exchangers by Cutting and Bending the Surface Layers," Novosti Teplosnab., No. 4, 51–53 (2005).
13. N. N. Zubkov and S. E. Shashkov, "Obtaining Enhanced Boiling Surfaces Using the Deforming Cutting Method," in *Proceedings of the All-Russia Scientific-Technical Conference "Machinery Construction Technologies," Bauman Moscow State Univ., Moscow, 2008.*
14. P. Thors and N. Zoubkov, "A Method and Tool for Making Enhanced Heat Transfer Surfaces," European Patent No. EP1692447, European Patent Bulletin, No. 34 (2006).
15. D. N. Morskoi, "Boiling Processes on Surfaces Obtained Using the Deforming Cutting Method," in *Proceedings of the All-Russia Conference of Young Scientists and Specialists "The Future of Machinery Construction in Russia*," Moscow, September 22–25, 2010 (Bauman MGTU, Moscow, 2010), pp. 163–164.
16. D. N. Morskoi and A. A. Yakomaskin, "Use of Microfinning in Two-Phase Thermosiphons," in *Proceedings of the 18th School-Seminar of Young Scientists and Specialists Led by the Academician of the Russian Academy of Sciences A.I. Leont'ev* "Problems of Gas Dynamics and Heat and Mass Transfer in New Power Technologies," Zvenigorod, May 23–27, 2011 (MEI, Moscow, 2011), pp. 201–202.
17. Yu. F. Gortyshov, I. A. Popov, N. N. Zubkov, et al., "Boiling of Water on Microstructured Surfaces," Trudy Akadenenergo, No. 1, 14–31 (2012).